Microsyst Technol (2017) 23:2577–2585
DOI 10.1007/s00542-016-3034-9

TECHNICAL PAPER

Analysis of effective vibration frequency of cable-driven parallel robot using mode tracking and quasi-static method

Hyun-Dong Do[1] · **Kyoung-Su Park**[1]

Received: 21 March 2016 / Accepted: 16 June 2016 / Published online: 23 June 2016

Abstract Recently, cable-driven parallel robots (CDPRs) have been used in many industry applications because of many advantages such as large workspace, high moving sensitivity and so on. In this paper, finite element model (FEM) including cables and end-effector was constructed and the pre-stressed modal analysis was carried out to obtain the natural frequencies. It was verified based on experimental results in order to investigate the effective frequency that most affects the dynamics of the end-effector. Two frequency response function (FRF) test results showed the vibration of end-effector was affected by the transversal vibration of cable. The effective frequency was extracted and investigated under asymmetric tension conditions using mode tracking and quasi-static method while the end-effector moves according to pre-programmed route. As a result, the minimum effective frequency occurred at the limit of the CDPR's motion, and was shown to be approximately a third of the maximum effective frequency. Total vibration amplitude of the minimum effective frequency was about three or four times larger than that of the maximum frequency.

1 Introduction

Cable-driven parallel robots (CDPRs) are a type of parallel manipulator in which the end-effector is supported in parallel by a number of cables, controlled by multiple actuators. CDPRs consist of three main parts: an end-effector, cables, and actuators (including winches). Generally, CDPR are categorized as fully constrained and under constrained. Fully constrained CDPRs require $n + 1$ cables, where n is the number of degrees of freedom (DOF) to be constrained (Riechel and Ebert-Uphoff 2004; Pham et al. 2009; Alexandre et al. 2012).

CDPRs have many advantages such as high moving sensitivity, a large workspace, transportability, and so on. Because of these advantages, CDPRs have recently been used in many industry applications such as portable cranes (Tadokoro et al. 1999), cameras (Wei et al. 2015), manufacturing tasks (Bostelman et al. 2000), virtual sports training systems (Morizono et al. 1997), and robotic surgery (Miyasaka et al. 2015). However, because the cables are only to be stretched but not compressed, it is difficult to control the position of end-effector of CDPR accurately. In addition, because they are inevitably flexible and vibrate in both axial and transversal directions, the vibration of end-effector connected to the cable caused by cable flexibility has been a concern for some applications which require high stiffness or high accuracy (Diao and Ma 2009). And vibration of end-effector can be excited by each cable vibration in both axial and transversal directions. However, most researchers usually modeled CDPR system by assuming each cable as an axial spring without considering its transversal vibration (Khosravi and Taghirad 2011; Yuan 2015; Ottaviano et al. 2015).

Diao and Ma (2009) analyzed the vibration of a cable-driven parallel manipulator by using cable with both the axial and transversal flexibility. And they concluded that internal forces in cables increased the natural frequencies of the transversal vibration of cables but almost not affected the vibration of the end-effector. However, his investigation only assumed a symmetric system (e.g.,

✉ Kyoung-Su Park
pks6348@gachon.ac.kr

[1] Department of Mechanical Engineering, Gachon University, 1342 Seongnamdaero, Sujeong-gu, Seongsam-si, Gyeonggi-do 461-701, Korea

symmetric positions and the same cable tensions) of the CDPR. As a result, all cables in the research had the same stiffness in all directions. Therefore, the vibration of cables was canceled out by the symmetric conditions applied in the study. However, it is largely different from real CDPR operating conditions, with respect for asymmetric tension and asymmetric stiffness of each cable. For example, when the end-effector is located at the corner of CDPR workspace, the natural frequencies are much larger than those in the center because of change of total stiffness (Williams II et al. 2008; Yuan 2015). Then, the shortened cables have too high stiffness, but the stretched cables have too low stiffness relatively. Therefore, because the natural frequencies of cables with low stiffness are low, they can be more easily excited than cables with high stiffness. So, if the external disturbances such as wind and friction in a temporary location (Shirato and Nishizaki 1995; Zen and Muftu 2003; Zen 2004) apply to the CDPR system through the cable, the accuracy of end-effector can be largely affected due to characteristics of cables vibration. Therefore, the effective frequency that most affects the vibration of the end-effector should be investigated for both directions, especially transversal direction as well as various positions.

Liu et al. (2002) reported that the transversal deflection of cables was observed in experiments, especially when the manipulator was in a high-speed or high-acceleration motion. However, he did not quantitatively investigate how much the transversal flexibility of cables contributes to the overall vibration of an end-effector.

The stiffness of a cable manipulator is one of the most critical ones because unexpected cable vibration always occurs due to the cable flexibility. However, effective frequencies obtained through frequency response function (FRF) test are better measurement of the degree of the stability of the end-effector of CDPR in terms of the vibration and accuracy.

In this paper, the effective frequency that most affects the dynamics of the end-effector is investigated under asymmetric tension condition while the end-effector moves according to pre-programmed route. To extract and track the effective frequency during motion of the end-effector, a 6-DOF CDPR is modeled using the ANSYS finite element tool. To verify the finite element model (FEM) of 6-DOF CDPR, the end-effector and cable vibration in the 6-DOF CDPR are measured using a Laser Doppler Vibrometer (LDV). The constructed FEM is verified with the experimental results. Using the verified FEM, the change of effective frequency is tracked under conditions of asymmetric tension by using mode tracking and quasi-static method. And the amplitudes of cumulated vibration in maximum and minimum effective frequencies are investigated quantitatively in order to evaluate the vibration characteristics for effective frequency.

2 Experiment set-up and FE modeling

2.1 Experiment set-up

This study used a 6-DOF CDPR system with eight cables, as shown in Fig. 1a. The coordinate of pulleys are summarized in Table 1. The frame size is 2 m × 2 m × 2 m (length × width × height), and the weight of end effector is 0.4 kg. Pulleys located asymmetrically were used to prevent the cables, which are connected to the end-effector, from interfering with each other during motion of the end-effector.

Fig. 1 A 6-DOF CDPR system

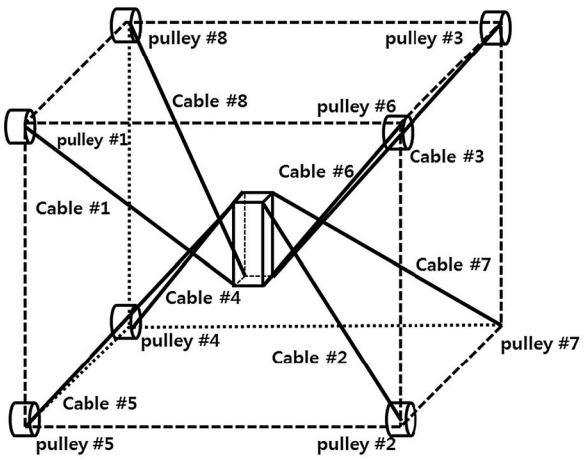

(a) Schematic of a 6-DOF CDPR

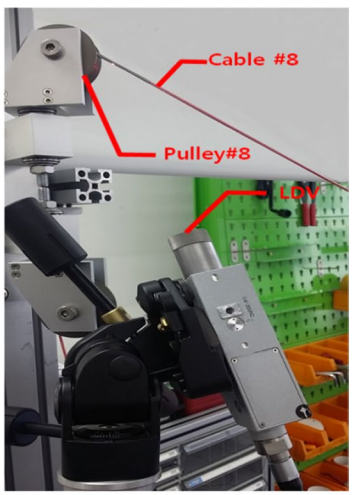

(b) Experiment set-up measuring cable vibration

Table 1 Coordinates of pulley location

No.	X (m)	Y (m)	Z (m)
Pulley 1	−0.930	−0.850	1.771
Pulley 2	0.840	−0.940	0.423
Pulley 3	0.930	0.850	1.771
Pulley 4	−0.840	0.940	0.423
Pulley 5	−0.835	−0.935	0.423
Pulley 6	0.95	−0.85	1.771
Pulley 7	0.835	0.935	0.423
Pulley 8	−0.950	0.850	1.771

Table 2 Three kinds of tension sets for equilibrium

Cable number	Tension set #1 (*N*)	Tension set #2 (*N*)	Tension set #3 (*N*)
Cable 1	10.25	14.52	11.50
Cable 2	2.16	7.84	2.00
Cable 3	10.25	14.52	11.50
Cable 4	2.72	7.84	3.12
Cable 5	7.55	11.98	8.70
Cable 6	1.27	7.24	2.23
Cable 7	7.28	10.97	8.50
Cable 8	2.16	4.54	2.60

Two kinds of experiments were carried out to verify the simulation model. The first experiment was conducted to measure the natural frequencies of the cable. Cable 8 was used for this experiment, as shown in Fig. 1b. Because of the light cable weight, a general vibration sensor, such as an accelerometer, couldn't be used in this work, and the cable vibration was measured with an LDV. In addition, because the Dyneema cable has a low reflectivity, it was wrapped with a highly reflective tape as shown in Fig. 1b. The time histories of signals measured by the LDV in cable 8 were recorded with a frequency of 100 Hz and sample rate of 1600 Hz, which was then filtered with exponential window when applying a transversal impulse input to cable 8. Because the proposed CDPR is the redundant actuated system, it can have many kinds of tension sets for static equilibrium. In the experiment, we used two other cable tension sets in order to investigate the tension effect. They were measured with load-cell on the pulley. One has low tension set on the whole. The other has higher tensions for equilibrium. They are summarized in Table 2.

Second, to measure the effective frequency of the end-effector, highly reflective tape was attached to the end-effector. For the center position of the end-effector (0 m, 0 m, 1.097 m), the vibration of the end-effector vibration was measured by applying a transversal impulse input to cable 8. The transfer function with input and output signals was measured with a frequency of 100 Hz and a sample rate of 1600 Hz, and was then filtered with a hamming window.

2.2 FE modeling

Figure 2a, b shows the FEM using ANSYS parametric design language (APDL). In the FEM, all cables were modeled with the link 10, which is a three-dimensional spar element having the unique feature of bilinear stiffness matrix resulting in a uniaxial tension-only element (Wei et al. 2012; Ren and Peng 2004). The cable material is polyethylene (Dyneema SK78). The FEM and material properties used in this research are summarized in Table 3.

For the cable vibration analysis, one side of the cable, which was connected with pulleys, was fixed for all other degrees of freedom in FEM. The other side was connected to the end-effector, which was modeled using Solid 45 element. Figure 2b shows the meshed model used in the

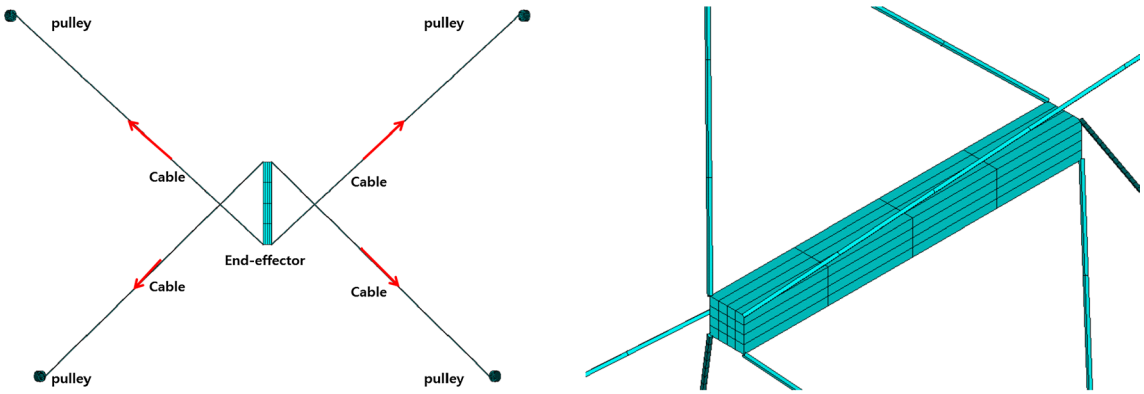

(a) FEM of a 6-DOF CDPR **(b)** meshed FEM

Fig. 2 FEM of a 6-DOF CDPR and meshed model

CDPR vibration analysis. In the FEM, the cables were divided into 20 elements, and the end-effector was divided into 16 elements. Because this research focuses on only the end-effector vibration induced by cable vibration, consider low order frequencies of cables, and does not consider the deformation of the end-effector, the number of cable element can describe the mode shapes significantly and number of end-effector elements is not vital. And the tension sets applied to the cable used with measured tension sets in the FE analysis.

3 Verification of the FEM and extraction of the effective frequency

3.1 Verification of the FEM

Figure 3 shows the measured natural frequencies of cable 8, where the position of the end-effector was centrally located, and asymmetric tensions were applied to the system (see Table 2). The tension values of cables were measured using a force sensor mounted on the pulley (load-cell, UMM-K200), for each experiment. As shown in Fig. 3, for cable tension set 1, the 1st and 2nd frequencies of cable 8 are 8.50 Hz and 16.63 Hz. For set 2, the 1st and 2nd frequencies are 13.31 Hz and 26.75 Hz. The results showed that the higher internal tension is, the higher natural frequencies have (Diao and Ma 2009). Also, the result can be explained by Eqs. (1) and (2).

$$c^2 \frac{\partial^2 u(x,t)}{\partial x^2} = \rho \frac{\partial^2 u(x,t)}{\partial t^2}, \quad c = \sqrt{\frac{T}{\rho}} \tag{1}$$

$$\omega_n = \frac{n\pi}{l}\sqrt{\frac{T}{\rho}} \tag{2}$$

In general, assuming a cable is fixed at both ends, stretched under tension, and deflects within its linear elastic range, the wave equation governing the free transversal vibration of the cable can be described by Eq. 1, where *u(x,t)* is the transversal displacement of the cable; *c* is the velocity of the wave propagation; *T* is the tension in the cable; and ρ is the mass per unit length of cable. Based on the above assumed boundary conditions, the natural frequencies to the transversal vibration modes of the cable can be described with Eq. (2). In the Eq. (2), the natural frequencies depend on the cable tension T. Therefore, the natural frequency is increased with increased cable tension.

With the constructed FEM and measured tension sets, the modal analysis was carried out.

The dynamic equilibrium equation of the model can be derived as follows;

$$[M]\{\ddot{u}\} + [C]\{\dot{u}\} + [K]\{u\} = \{F(t)\} \tag{3}$$

where $[M]$, $[C]$ and $[K]$ are the mass matrix, damping matrix, stiffness matrix of the total system, respectively. And $\{u\}$ represents the displacement vector of each node. Then, applied tension makes cable stretched. Under pretension, the elongation of flexible cable can be derived as follows;

Table 3 Material properties of the cable and end-effector

Name	Cable	End-effector
Element	Link10	Solid 45
Material	Dyneema SK78	Stainless steel
Area	6.25×10^{-6} m^2	0.9×10^{-3} m^2
Elastic modulus	19.2 Gpa	200 Gpa
Poisson's ratio	–	0.29
Density	510 kg/m^3	1484 kg/m^3

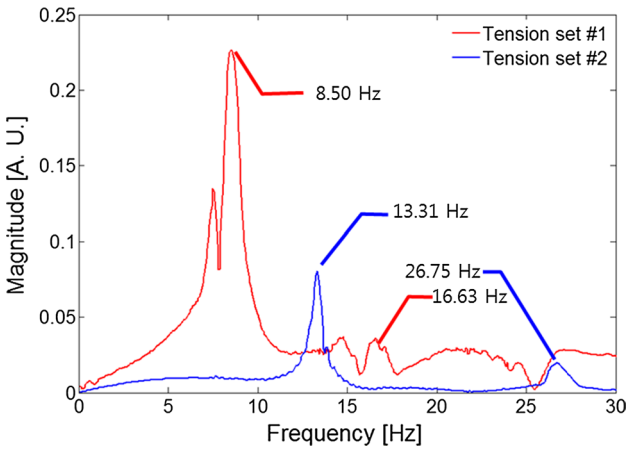

Fig. 3 Measured natural frequencies of cable 8

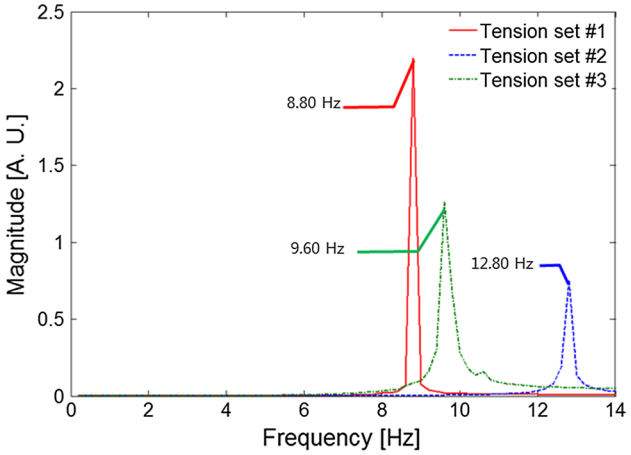

Fig. 4 Calculated natural frequencies of cable 8 with FEM

Table 4 Comparison between the experiment (EXP) and FEM results

	Tension set #1 (Hz)		Error (%)	Tension set #2 (Hz)		Error (%)
	EXP	FE		EXP	FE	
1st	8.5	8.8	3.5	13.3	12.8	3.8
2nd	16.6	17.7	6.6	26.8	25.6	4.5

$$[\tilde{K}]\{u\} = -\{T\} \tag{4}$$

where $\{T\}$ means the applied cable tension and $[\tilde{K}]$ is the flexibility matrix. Let $\{u\} = \{\Phi\}e^{j\omega t}$, and the differential equation can be solved by ignoring the resistance for free vibration condition,

$$(-\omega^2[M] + [K + \tilde{K}])\{\Phi\} = 0 \tag{5}$$

We can obtain the characteristic equation for the system and calculate natural frequencies of the system and vibration mode shapes of the system from Eq. (5). In Eq. (5), the pre-stressed force makes total system stiffened. As a result, it increases the natural frequency of the system.

Therefore, the pre-stressed modal analysis was performed in this research by considering the stiffening effect induced from the internal cable stresses in FE analysis. To do this, linear static analysis of CDPR cable was first carried out with a tension set, obtained through experimentation. The internal stress induced by the deformation of cable was then calculated, and block Lanczos modal analysis was performed by considering stiffening effect at cable. The block Lanczos method is recognized as a more effective tool for extraction of structural mechanics (Fialko et al. 2003). Figure 4 shows the calculated natural frequencies with tension set. And Table 4 summarized the results of simulations and experiments. As shown in Table 4, the simulation closely agrees with the experimental results under approximately 7 %. That means the constructed FEM was suitable for the dynamic analysis of the proposed CDPR. Figure 5 shows the 1st mode shapes of the cable when the end-effector was located at (0, 0, 1.097 m) and asymmetric tension was applied to each cable. The 1st mode shape had two nodal points in cable 8. They generally corresponded to the cable mode shape.

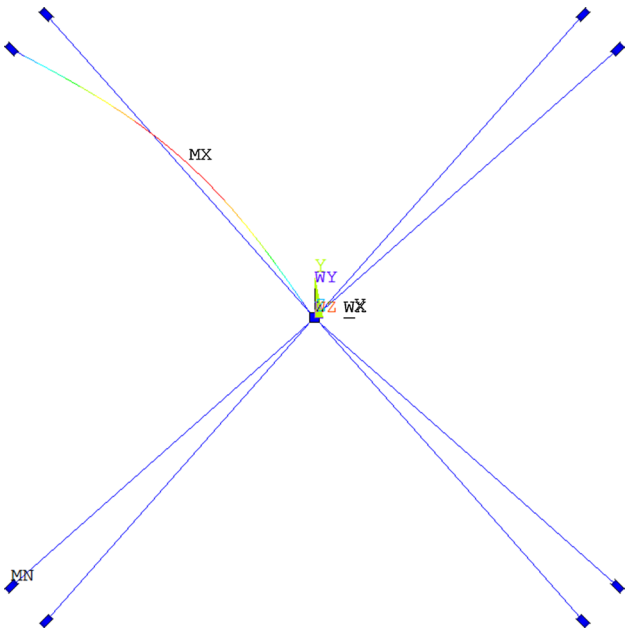

Fig. 5 Mode shape for 1st frequencies

Figures 6 and 7 show the mode shapes of total CDPR cables for two cases of the center and the corner position of end-effector. As shown in the figures, the mode shapes at the center position are different from those at the corner position. In the center, the mode shapes generally consist of the first mode of a single cable or the combination of first mode of some cables up to 12th mode. However, the mode shapes become too complex when the end-effector is located at the corner of the frame (see Table 5). Some mode shapes consist of combination of 1st mode of a single cable and 2nd or 3rd mode of other cable. The different mode shapes inform what the dominant cable is in the frequency.

3.2 Extraction of the effective frequency of the end-effector

Figure 8 shows the measured FRF of the end-effector vibration for an end-effector position of (0, 0, 1.097 m) when applying tension set 3 to all cables and inducing an impulse to cable 8. This allowed the effective frequency of multiple cable vibration modes to be extracted. In Fig. 8, a frequency of 7 Hz was analyzed as the structural frequency (the frame and pulley coupled frequency) regardless of end-effector and cable vibration. In the comparison between Figs. 4 and 8, both showed similar results for the first fundamental frequency (9.51 Hz) of the cable. Also, a harmonic frequency (19.24 Hz) was seen. This suggests that the dynamics of the end-effect was affected by the cable's transverse vibration modes.

This research considered high acceleration conditions, up to 100 m/s^2. The main stimulated frequency during the CDPR operation could be calculated as 10 Hz. Therefore,

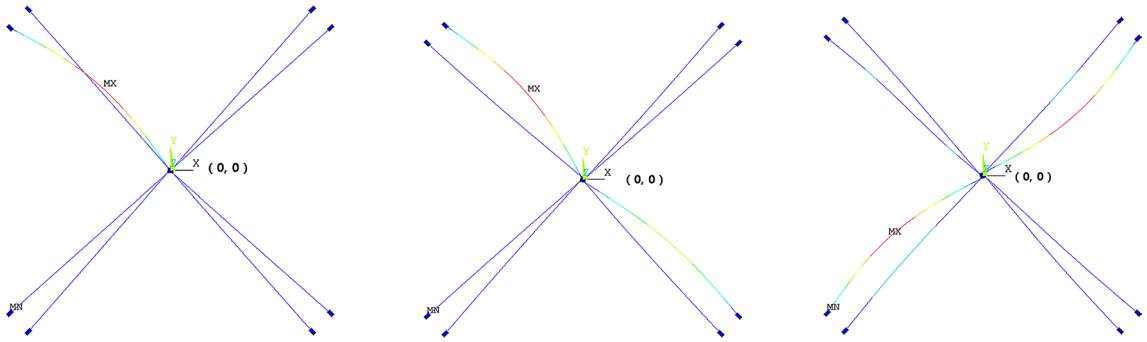

(a) 12.71 Hz **(b)** 16.51 Hz **(c)** 23.28 Hz

Fig. 6 Various mode shapes of cable of CDPR (at the *center*)

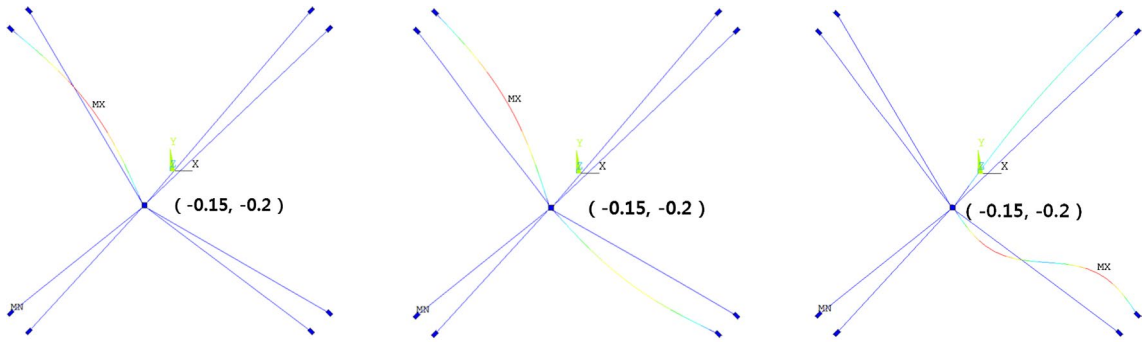

(a) 4.21 Hz **(b)** 11.71 Hz **(c)** 17.70 Hz

Fig. 7 Various mode shapes of cable of CDPR (at the *corner*)

Table 5 Mode shapes with position of end-effector (at the center and corner)

No.	Center		Corner	
	Frequency (Hz)	Note (cable number)	Frequency (Hz)	Note (cable number)
1st	12.71	#8 (1st)	4.21	#8 (1st)
2nd	12.76	#8 (1st)	8.45	#8 (2nd)
3rd	15.77	#2, #4, #6 and #7 (1st)	8.82	#6 (1st)
4th	16.12	#6 (1st)	11.71	#2 and #4 (1st)
5th	16.51	#4 and #6 (1st)	11.79	#4 (1st)
6th	16.74	#4 (1st)	11.80	#2 and #4 (1st)
7th	19.54	#2 (1st)	11.81	#4 (1st)
8th	19.84	#7 (1st)	12.75	#8 (3rd)
9th	20.12	#1, #2, #3, #5 and #7 (1st)	16.55	#3 (1st)
10th	20.73	#5 (1st)	16.92	#3 and #7 (1st), #6 (2nd), #8 (3rd)
11th	21.02	#1, #2, #3, #5, #6 and #7 (1st)	17.14	#8 (4th)
12th	22.83	#1 and #3 (1st)	17.16	#3 and #7 (1st), #8 (4th)
13th	23.28	#1, #3, #5 and #7 (1st), #8 (2nd)	17.57	#7 (1st)

this research considered frequencies up to approximately 15 Hz. The effective frequencies were mostly determined from the 1st cable frequencies under these operating conditions. The dynamics of the end-effector could be affected by vibrations of the cable in the real CDPR, and the stiffness of each cable was different due to varying

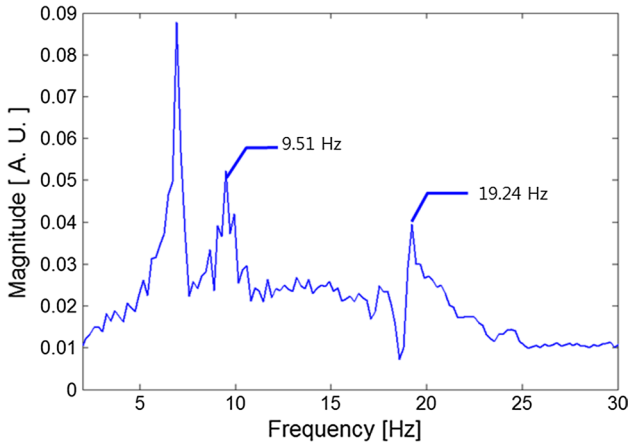

Fig. 8 Measured effective frequencies of the end-effector

cable lengths and tensions. Although the CDPR forces reached equilibrium, the end-effector vibrated due to differences in asymmetric vibration energy when an external disturbance was applied to the CDPR system.

3.3 Tracking of the effective frequency

The end-effector moved according to a pre-programed route, which then applied the tension thereby resulting in an asymmetric system (see Fig. 9). Two speeds were used; low speed (0.026 m/s); and high speed (0.26 m/s). In this experiment, the z-height was maintained, and the end-effector periodically moved in the x- and y-directions. The x and y ranges were ±0.2 m. It was difficult to analyze the vibration characteristics over the full time-scale, as this required high computational power. Therefore, this work performed quasi-static analysis. This was possible because, when the dynamic forces were applied, the controller attempted to make the system equalize resulting in distributed optimal tensions. The applied tensions measured in this experiment were dynamic forces. The simulation used these tensions as the tension set. And Fig. 9 shows the measured tension profiles of each cable while the end-effector moves according to the pre-programed route. In the simulation, the tensions were applied to the cables. The mode tracking method was used to search for the effective frequency, as the order of effective modes could be changed while the end-effector continuously moved. Figure 10 showed the simulation results, which are the product of variation of the effective frequency during the pre-programmed route. In Fig. 10, the red bold, blue and green lines represent the variation of effective frequency, y-direction, x-direction motion, respectively.

Figure 10 shows the variation of the effective frequency for two cases (low and high speed); as can be seen in the figure, effective frequency varied widely. In this research, the workspace was chosen as ± 0.2 m to exclude any unstable dynamics. Although the end-effector moved within a small range (±0.2 m), the variation in frequency was 4.2 to 13.2 Hz, i.e., the difference could approach up to 300 %. This is because the total stiffness was mainly affected by extension, rather than shortening, of the cable during motion of the end-effector. When the cable was shortened, it did not vibrate, but vibration was seen when it was extended. Therefore, the minimum effective frequency occurred at the limit of the end-effector's motion. A low effective frequency may result in an unstable CDPR system when considering the natural frequencies (under 7 Hz) of the frame and pulley. Therefore, the simulation used to investigate the variation of the effective frequency was very important, especially within a large workspace. The trend is similar for both the low and high speed cases. It can be seen in Fig. 10 that, even though the position of the end-effector was not altered, the effective frequency is slightly

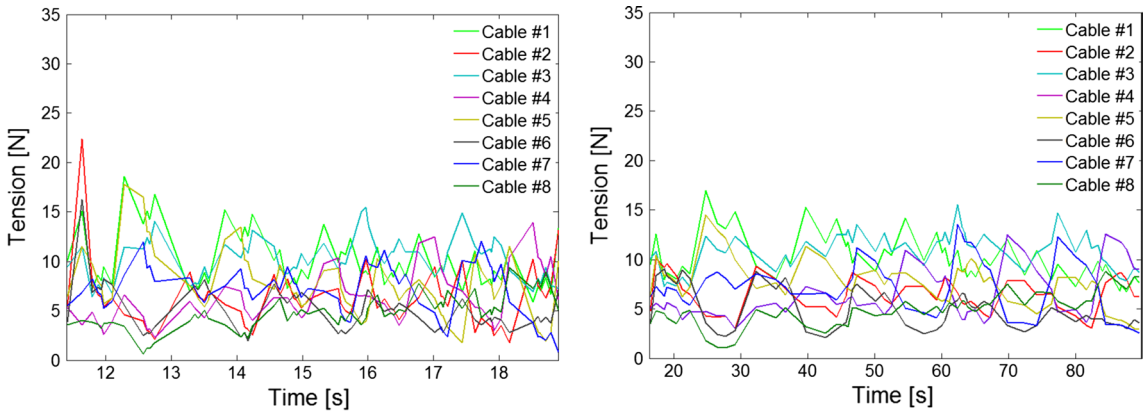

(a) Speed of 0.26 m/s

(b) Speed of 0.026 m/s

Fig. 9 Measured tension profiles while the end-effector moves

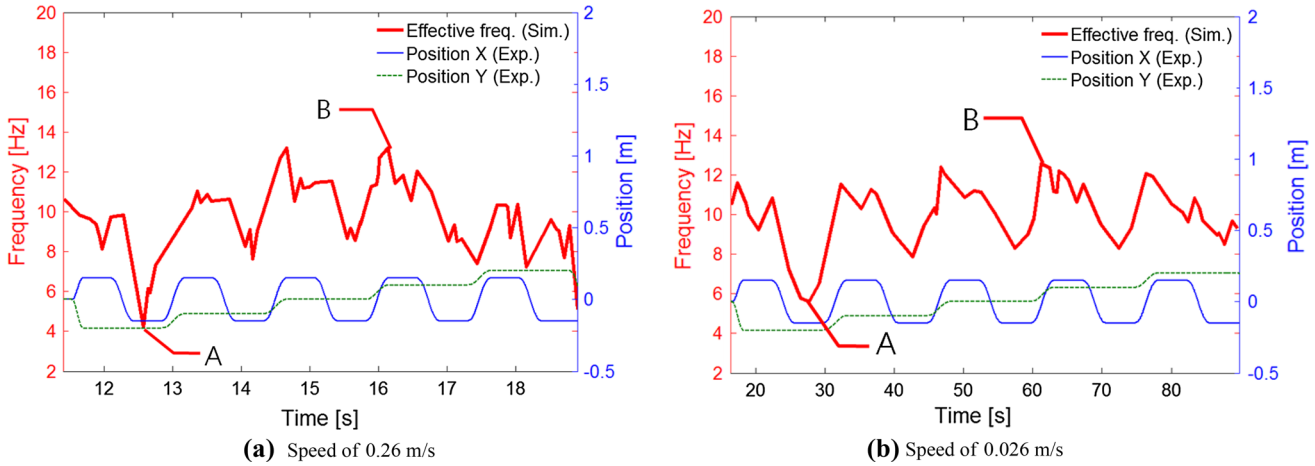

(a) Speed of 0.26 m/s **(b)** Speed of 0.026 m/s

Fig. 10 Tracking of the effective frequency with position and tension

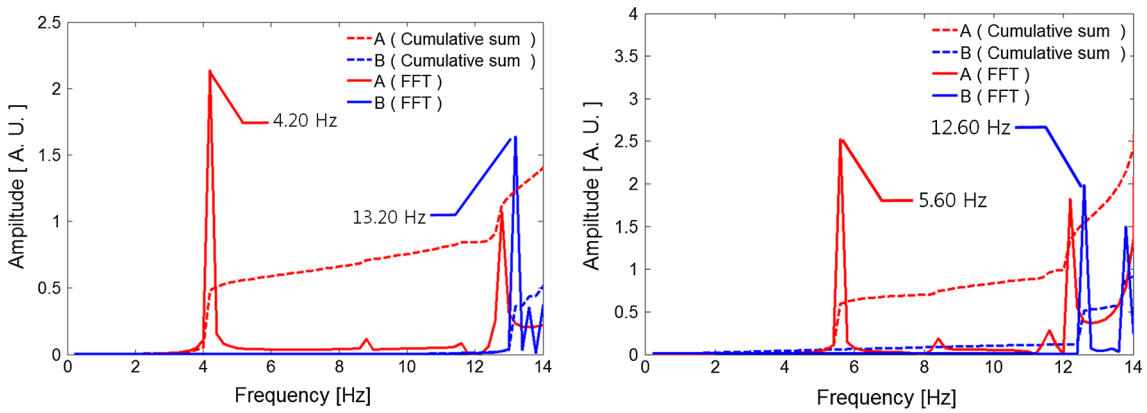

(a) Speed of 0.26 m/s **(b)** Speed of 0.026 m/s

Fig. 11 Harmonic analysis results and amplitudes of cumulated vibration in the maximum and minimum effective frequencies

changed. This phenomenon is due to asymmetric tension in the pre-programed position used.

Figure 11 shows the harmonic analysis results of the minimum (A) and maximum (B) frequencies shown in Fig. 10. In the figure, the red line represents the effective frequency and cumulated vibration amplitude of the minimum frequency (A). And the blue is the effective frequency and cumulated vibration amplitude of the maximum frequency (B). A cumulative sum was performed to analyze the amplitude of vibration of the end-effector in the frequency domain. In the figure, the dotted lines show the cumulative sum, in which the amplitude of vibration is integrated in the frequency domain. From these results, it ca be seen that the amplitude of the minimum effective frequency is five times larger than that of the maximum effective frequency. The trend is also similar at low speeds. As a result, the accuracy of the end-effector can vary widely according to the cable vibrations that occur when the end-effector moves. The frequency was at its lowest when any of the end-effector's positional co-ordinates were close to zero. When this happened, the length of the cable was asymmetric. When the cables had an asymmetric length, there were increased vibrations. The workspace and stiffness should therefore be analyzed in CDPRs. Also, it is highly important that variations in the effective frequencies and total vibration amplitude are analyzed.

4 Conclusions

In this paper, an analysis of the vibrations of CDPRs was investigated. First, an FEM was constructed and verified based on experimental test results. The constructed FEM of the CDPR was shown to be suitable for analyzing the variation of the effective frequency while the end-effector moved. The effective frequency was extracted and

investigated under asymmetric tension conditions using mode tracking and quasi-static method while the end-effector moves according to pre-programmed route. As a result, the minimum effective frequency occurred at the limit of the CDPR's motion, and was shown to be approximately a third of the maximum effective frequency. The amplitude of the minimum effective frequency was about three or four times larger than that of the maximum frequency.

Acknowledgments This research was supported by Leading Foreign Research Institute Recruitment Program through the National Research Foundation of Korea (NRF) funded by the Ministry of Science, ICT & Future Planning (MSIF) (2012K1A4A3026740) and this research was supported by Basic Science Research Program through the National Research Foundation of Korea (NRF) funded by the Ministry of Science, ICT & Future Planning (2015037574).

References

Alexandre DSJ, Daney D, Gouttefarde M (2012) Calibration of a fully-constrained parallel cable-driven robot in ROMANSY 19th CISM-IFToMM symposium on robot design, dynamics and control, pp 1–8

Bostelman R, Jacoff A, Proctor F, Kramer T, Wavering A (2000) Cable based reconfigurable machines for large scale manufacturing. Proceedings of the 2000 Japan-USA Symposium on Flexible Automation, pp 23–26

Diao X, Ma O (2009) Vibration analysis of cable-driven parallel manipulators. Multibody Syst Dyn 21:347–360

Fialko SY, Kriksunov EZ, Karpilovsky VS (2003) A block lanczos method with spectral transformations for natural vibrations and seismic analysis of large structures in SCAD software. Proceedings of the CMM-2003-computer Methods in Mechanics. June 3–6

Khosravi MA, Taghirad HD (2011) Dynamic analysis and control of cable driven robots considering elasticity in cables. CCToMM M^3 Symposium, pp 1–12

Liu J, Ning K, Zhao M (2002) Model of a new type wire driven parallel robot system. J Northeast Univ 23:988–991

Miyasaka M, Matheson J, Lewis A, Hannaford B (2015) Measurement of the cable-pulley coulomb and viscous friction for a cable-driven surgical robotic system. Intell Robot Syst, pp 804–810

Morizono T, Kurahashi K, Kawamura S (1997) Realization of a virtual sports training system with parallel mechanism. IEEE Int Conf 4:3025–3030

Ottaviano E, Gattulli V, Potenza F (2015) Modeling a planar point mass sagged cable-suspended manipulator. The 14th IFToMM World Congress: WC.OS2.050

Pham CB, Yeo SH, Yang G, Chen IM (2009) Workspace analysis of fully restrained cable-driven manipulators. Robotics Autonomous Syst 57:901–912

Ren W, Peng X (2004) Baseline finite element modeling of a large span cable-stayed bridge through field ambient vibration tests. Comput Struct 83:536–550

Riechel AT, Ebert-Uphoff I (2004) Force-feasible workspace analysis for underconstrained, point-mass cable robot. Robotics Automation 5:4956–4962

Shirato H, Nishizaki T (1995) Response characteristics of rain-wind induced vibration of stay-cables of cable-stayed bridges. Journal of wind engineering 57:323–333

Tadokoro S, Verhoeven R, Hiller M, Takamori T (1999) A portable parallel manipulator for search and rescue at large-scale urban earthquakes and an identification algorithm for the installation in unstructured environments. Intell Robots Syst 2:1222–1227

Wei L, Cheng H, Li J (2012) Modal analysis of cable-stayed bridge. Int Conf Adv Comput Model Simul 31:481–486

Wei H, Qiu Y, Yang J (2015) An approach to evaluate stability for cable-based parallel camera robots with hybrid tension-stiffness properties. Adv Robot Syst, pp 1–12

Williams II RL, Xin M, Bosscher P (2008) Contoure-crafting-cartesian-cable robot system concepts: workspace and stiffness comparisons. ASME 2008 International Design Engineering Technical Conference, pp 1–8

Yuan H (2015) Static and dynamic stiffness analysis of cable-driven parallel robtos. These INSA Rennes

Zen G (2004) Friction induced transverse vibrations of an axially accelerating continuum. Master of Science Thesis, Northeastern University

Zen G, Muftu S (2003) Friction induced transverse vibrations of an axially accelerating string. Proceedings of STLE/ASME Int. Joint Tribology Conference:TRIB-262